

Enhancement of stability delay margins by virtual inertia control for microgrids with time delay

Suud Ademnur HASEN^{1,2}, Şahin SÖNMEZ^{2,*}, Saffet AYASUN¹

¹Department of Electrical and Electronics Engineering, Faculty of Engineering, Gazi University, Ankara, Turkey

²Department of Electronics and Automation, Yeşilyurt Vocational High School, Malatya Turgut Özal University, Malatya, Turkey

Received: 07.03.2022

Accepted/Published Online: 29.07.2022

Final Version: 28.09.2022

Abstract: Large-scale deployment of renewable energy sources (RESs) contributes to fluctuations in the system frequency due to their inherent reduced inertia feature. Time delays have emerged as a major source of concern in microgrids (MGs) as a result of the broad adoption of open communication networks since significant delays inevitably reduce the controller's performance and even cause instabilities. In this article, a frequency-domain direct method is used to evaluate the impact of the virtual inertia (VI) control on the stability delay margins of MG with communication delays. By avoiding approximation, the approach first removes transcendental terms from characteristic equations and turns the transcendental characteristic equations into regular polynomials. With this method, roots of the original characteristic equation on the imaginary axis correspond to exactly the positive real roots of the new regular polynomial not including any exponential term. This new polynomial can be used to find out whether the system stability is delay-dependent or not and enables us to compute stability delay margin for the delay-dependent stability case. The proposed analytical method is utilized for evaluating stability delay margins with regard to system parameters for various values of proportional-integral (PI) gains where the MG is marginally stable. Moreover, quantitative effect of virtual inertia and damping gains is comprehensively investigated. Based on the results, it is concluded that incorporating VI control enhances stability delay margins and enhances the MG's stability performance. Theoretical delay margin results are verified using time-domain simulations and quasipolynomial mapping-based root finder (QPmR) algorithm.

Key words: Communication time delays, microgrids, renewable energy sources, stability delay margin, virtual inertia

1. Introduction

Escalating concerns over environmental effects caused by traditional power generation head to the high level penetration RESs such as solar and wind powers, and distributed generators (DGs) for instance small thermal power plant into power systems [1, 2]. The large-scale penetration of DGs/RESs reduces the number of traditional generating units that provide immediate preliminary response and reserve power for frequency management. However, it results in significant frequency fluctuations and weakens the system stability and resiliency. Additionally, due to the utilization of power electronics interfaces, DGs/RESs-based generation has no or extremely low inertia and damping [3].

There is no rotating mass in power-electronics interfaces, which is critical for providing inertia and damping qualities during a disruption. The deficiency of system inertia and damping cause an increase in the

*Correspondence: ssonmeztr@gmail.com

rate of change of frequency (RoCoF), resulting in sudden frequency fluctuations with bigger amplitudes and load-shedding perhaps even for minor disruptions. Excessive RoCoF may occur if generation entities are not built to ride through, resulting in cascaded tripping. If system inertia drops below a particular value, the huge generation drop will cause a swift frequency decrease; similar to what would happen in frequency load-shedding, consequential to instability, cascading outages, and power blackouts. Furthermore, power electronic circuits connected to nonsynchronous generators are instantly delivered into electrical grid as a power disturbance, causing in a momentous drop in system inertia, which has a major impact on frequency stability, dynamic performance, and reliability [1, 4]. Furthermore, the intermittent nature of RESs, which results in unanticipated power swings, affects the system's dynamic performance [4, 5].

Virtually synthesizing extra inertia and damping, sanctioning for substantial DGs/RESs contribution in system operation, is one strategy for stabilizing modern power systems in reaction to stability issues posed by system inertia and damping reduction [6–8]. Different topologies have been suggested to simulate virtual inertia [1, 4]. These topologies are all based on the same foundation. However, the level of precision with which they are implemented varies. Virtual inertia emulation topologies can be classified into three categories: i) *Synchronous generator model – based topology* mimics virtual inertia based on complete model of synchronous generator (SG) dynamics, such as the virtual synchronous machine (VISMA) [6] and synchronverter [8]. The dynamics of an SG are accurately duplicated since both electrical (e.g., winding interaction) and mechanical (i.e. rotational mass and inertia) components of SG are represented. ii) *Swing equation – based topology* mimics virtual inertia according to the SG's swing equation such as Ise Lab's topology [9] and synchronous power controller (SPC) [10]. Hence, only the swing equation is modelled rather than the entire SG to imitate virtual inertia. iii) *Frequency – power response – based topology* emulates virtual inertia according to the reaction to the frequency changes such as virtual synchronous generator (VSG) [7]. Here, the topology utilizes derivative of the frequency change measurement to imitate the virtual inertia. Among the numerous ways outlined above, the virtual emulation based on RoCoF of the system is chosen in this article since it is the easiest and very basic method for simulating virtual inertia.

The insufficient inertia and damping due to the high level integration of RESs into MG systems have attracted considerable attention in recent years. Authors in [11] proposed an adaptive control technique for tuning controller gains of the interconnected two-area MG system supported by batteries of electric vehicles (EVs) and VSG. The study reported in [12] analyzed the robustness of the MG frequency control system for the tuned VSG parameters using a quantitative feedback theory against load disturbance events and power fluctuations in RESs. The study in [13] proposed a synthetic inertia technique based on EVs for providing synthetic inertia services in modern power grids with low inertia in the presence of system uncertainties, high integration levels of RESs and nonlinearities conventional power generations. Moreover, considering line impedances of the MG system, authors in [14] proposed a feedforward decoupling strategy based novel virtual inertia control to alleviate the low inertia problem of MG systems having power converters. The study presented in [15] reported a hierarchical control scheme based on a distributed controller design to improve the voltage and frequency stability in the AC/DC multi-area MG systems including VSG control. Finally, the paper in [16] developed a fuzzy logic controller based emulated inertia controller to estimate the requirement of the inertial power depending on the frequency deviation. Real-time simulation studies were performed to validate the effectiveness of proposed controller and to illustrate the superiorities of the proposed technique on the conventional emulated inertia control. The recent studies estimate the virtual inertia and damping

constants in MG systems by using various techniques and investigate the robustness of the grid frequency against uncertainties in RESs, parametric uncertainties of MG system and load variations.

Apart from diminished inertia, the communication time delays in MGs pose a significant threat to system stability. To manage control actions and maintain system stability and operation, the MGs are equipped with a variety of communication networks. The widespread use of communication networks for regulating system frequency and maintaining dynamical stability in modern power systems has been unavoidable with the advent of new control techniques in the frequency control service. Phasor measuring units (PMU) and open communication networks became widely employed in wide-area measurement/monitoring systems (WAMS). Consequently, time delays like measurement and transmission delays are unavoidable [17, 18]. When such time delays reach the upper bound called the stability delay margin, they are known to reduce damping performance of the control system and perhaps even lead to instability [19, 20]. Time delays linked to communication networks are generally disregarded in MG stability studies since dedicated networks with short delays are typically employed for sending data and control signals. Nevertheless, when open and distributed communication channels are employed in MGs, temporal delays of 5–15 s are seen [19, 20]. A variety of factors determine the size of communication delays. Telephone lines, power line carriers, fiber-optic cables, and other communication mediums, as well as network load, transmission protocol, and phasor package size, are all aspects to consider. Consequently, transmission delay within a particular range may vary at random. Hence, determining the delay margin is crucial in the stability study of time-delayed MGs. The capability to design a controller that assures system stability even when delays are uncertain is made possible by knowing delay margins.

There are various methods available to compute stability delay margins. These techniques are divided into two main groups: time-domain based indirect methods and the frequency-domain based direct methods. The time-domain indirect methods based on Lyapunov stability theory and linear matrix inequalities (LMIs) were applied to the delay margin computation of LFC systems not including VI control. It is well-known in the literature of the time-delayed systems that the time-domain indirect methods give conservative stability delay margins as compared to the frequency-domain direct method [21, 22]. The frequency-domain techniques aim to locate all crucial purely imaginary roots of the characteristic equation. Schur-Cohn method [23, 24], elimination of transcendental components from the characteristic equation [25], Rekasius substitution [26, 27] are among the most well-known and widely used frequency domain techniques for computing delay margin in power systems. In recent years, various studies have examined stability delay margins of several systems not including VI control such as MG LFC systems [28, 29], wind turbine systems [30], conventional LFC systems [31] and modern LFC systems enhanced by electric vehicles [32, 33] by using Rekasius substitution and direct method based on the elimination of exponential terms. From a computational point of view, when both methods are compared, Rekasius substitution has the following disadvantages: i) A pseudo-delay term must be introduced for exponential delay terms in the characteristic equation, ii) Routh-Hurwitz method must be applied to determine the purely imaginary roots and the corresponding delay margins, which requires significant computational effort [29, 33]. Because of these reasons, in this study, the direct method based on the elimination of exponential terms is utilized for delay margins computation. For time-varying delays, frequency domain techniques cannot be utilized to analyze the stability of time-delayed systems; instead, time-domain indirect approaches should be used. Even if exact delay margins for constant delays may be achieved, this is the downside of frequency domain direct techniques.

The effects of time delays in the demand response loop on system frequency response are examined using a modified LFC model of single-area power system that includes demand response and virtual inertia [34]. [35]

presented robust virtual inertia control for MG with low inertia to reduce unwanted frequency measurement delay impacts and improve MG frequency stability. A new virtual inertia control approach was developed in [36], which introduces a virtual damper to the existing virtual inertia control strategy to mitigate the effects of time delay caused by cyber-attacks on the isolated MG's LFC loop. Due to the single-phase structure of the grid and communication delays, [37] proposed the use of plug-in hybrid electric vehicles to stabilize frequency in MGs and/or weak grids with insufficient inertia. [38] presents a means for computing and correlating the upper limit on virtual inertia gain to the phase-locked loop low pass filter's cut-off frequency, which is used to represent the delay indirectly. The issue of developing a virtual inertia control system according to a robust model predictive controller that takes into account time delays in MGs was recently addressed in a new published article [39]. The literature (e.g., [37–39]) that considers virtual inertia and communication time delay has one or more of the following limitations: the stability delay margin is not computed, Padé approximation of time delay was utilized instead of the exact value, and the impact of allocating virtual inertia control and load disturbance in control area has yet to be quantified or compared. To the best knowledge of the authors, no study has been conducted to quantify the impact of virtual inertia parameters on stability delay margin computation of MGs with communication time delay, which is the main contribution of this article.

This article studies the impacts of virtual inertia parameters on stability delay margin, which designates the upper bound of time delay of the MG with VI control (MG-VI). The direct method calculates delay margins with regard to system parameters for wide range of the PI controller gains of the system. The stability delay margins of the system are then calculated to analyze the impact of inertia and damping parameters on stability and dynamics of the system. The verification of the accuracy of stability delay margin is investigated via time-domain simulations [40] and quasipolynomial mapping-based root finder (QPmR) algorithm [41] over a wide range of the PI controller gains. The results clearly reveal that with the integration VI control to the MG system, stability delay margins considerably increase, indicating that frequency stability is enhanced when compared to a MG system without VI loop.

2. Time-delayed MG-VI system model

Figure 1 depicts a schematic diagram of an islanded MG that contains microgrid central controller (MGCC), DGs/RESs, energy storage system (ESS), small-scale power plant, domestic loads and a VI model. The MGCC collaboratively controls all DGs/RESs and small power plant to maintain the system frequency and voltage in an acceptable range. Through communication networks represented by the dotted line in Figure 1, MGCC is responsible for the integrity and harmonization of the entire system. ESS is charged or discharged based on its state of charge (SOC), as shown by the bidirectional power flow. Domestic loads consume power in MGs, while DGs inject power. The solid line in Figure 1 indicates the power exchange between DGs, ESS, and domestic load groups.

Figure 2 shows a simplified dynamical model of an islanded MG system where the linearized models of each component are utilized. This model is based on [3] and is utilized to study the impact of VI on the system's stability, performance, and resilience. In this MG, generation units and their installed capacities are selected as solar power plant of 7.5 MW, wind power plant of 8.5 MW, and thermal power plant of 15 MW. In addition, the MG system has residential loads of 5 MW and commercial-industrial loads of 10 MW. Because of high-level penetration of power electronic devices connected to the MG, an ESS of 4.5 MW is added to the system taking to consideration the obstacles related to low inertia and insufficient damping of the system. The base power is 15 MW [3]. In the islanded MG, ΔP_m , ΔP_g , Δf , ΔP_v , ΔP_L and ACE are the deviations in mechanical

output of generator, governor output, frequency, the valve position and domestic load, respectively. T_g , T_t , T_{WT} , T_{PV} , M , D , R and β represent time constant of the governor and turbine, wind turbine, solar system, the inertia constant, damping coefficient, speed drop of the control area and frequency bias factor, respectively.

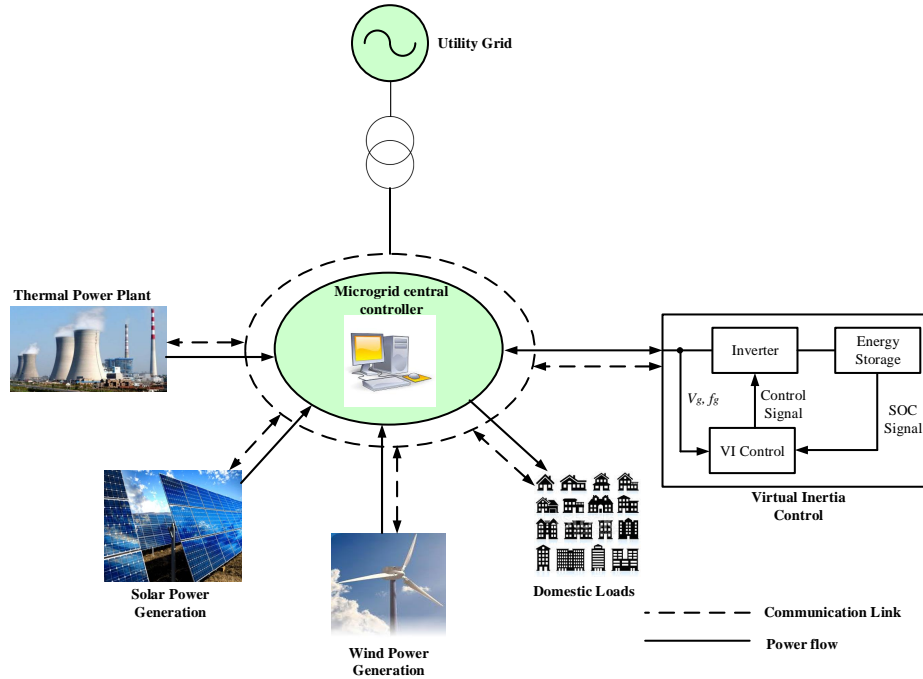


Figure 1. Schematic diagram of MG system.

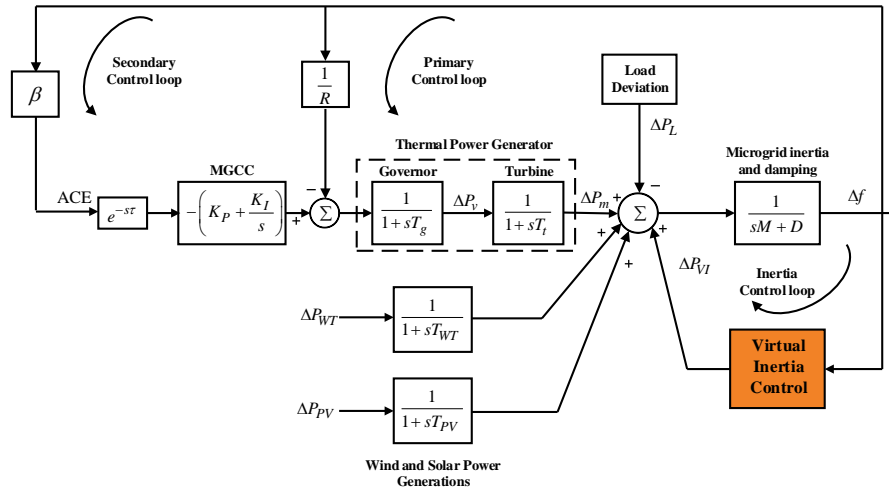


Figure 2. The dynamical model of islanded MG.

To control the frequency, Figure 2 demonstrates three distinct control level schemes named primary, virtual inertia, and secondary. The primary control loop of a small-scale thermal power plant conducts the initial control activity and controls the governor and synchronous generator inertia locally for frequency regulation. Second, an inertia control loop is used as a supplementary control to deliver virtual inertia and damping values

using the ESSs via a derivative control technique df/dt that mimics the prime mover’s behavior. Finally, the secondary control loop employs the load frequency control (LFC) mechanism to improve frequency stability and eliminate steady state error. Using the communication networks with low-bandwidth, MGCC transmits the area control error (ACE) signals to each DG to reinstate the system frequency. The total time delay resulted from receiving/transmit the control signals is expressed by an exponential term of $e^{-s\tau}$ in Figure 2. Proportional-integral (PI) controller is deployed by the MGCC as follows:

$$G_C(s) = K_P + \frac{K_I}{s} , \tag{1}$$

where K_P and K_I are the gains of MGCC PI controller. The dynamic model of the virtual inertia control system is displayed in Figure 3. The virtual inertia control system contains an energy supply, an inverter, and appropriate virtual inertia emulation control unit. Using the derivative technique described in [42, 43], the virtual inertia component is constructed by computing the RoCoF for adjusting the excess power to a set-point of the MG-VI system during a disturbance. The virtual damping component is utilized for a speedy settling/stabilization period according to the system’s frequency fluctuations. Consequently, the RoCoF is used to dynamically regulate active power using an inverter-based ESS. Thus, the MG-VI system is able to accurately simulate virtual inertia power with damping, enhancing system inertia, damping, and frequency stability. The basic algorithm of virtual inertia control governs the required inertia K_{VI} to be applied to the grid and provides the extra power transfer when the system frequency and RoCoF surpass a predetermined limit.

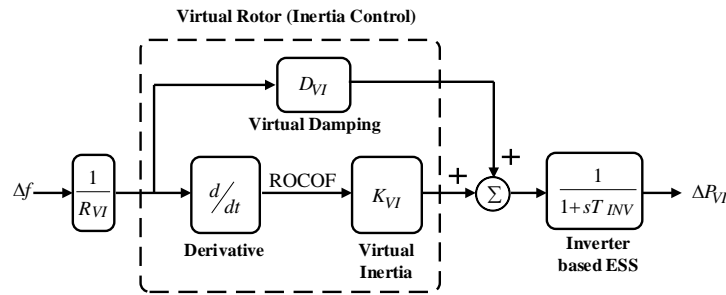


Figure 3. Dynamic frequency response structure for virtual inertia control.

$$\Delta P_{VI} = K_{VI} \left(d \frac{\Delta f}{dt} \right) + D_{VI} (\Delta f) , \tag{2}$$

where D_{VI} is the virtual damping constant and K_{VI} is the virtual inertia constant. To develop the dynamic model of virtual inertia control shown in Figure 3, the dynamic characteristics from (2) for mimicking virtual inertia and damping are merged as (i) inverter-based energy storage’s first order transfer function, and (ii) droop characteristic of virtual inertia. Hence, the dynamic equation [3, 5] can be used to express the virtual inertia power.

$$\Delta P_{VI}(s) = \frac{sK_{VI} + D_{VI}}{1 + T_{INV}} \left(\frac{\Delta f(s)}{R_{VI}} \right) , \tag{3}$$

where T_{INV} is the time constant of inverter-based energy storage and R_{VI} is the virtual inertia droop constant for regulating active power with regard to frequency control. Finally, using the linearized first-order transfer

functions, the characteristic equation of the MG with VI could be computed as follows:

$$\Delta(s, \tau) = P(s) + Q(s)e^{-s\tau} = 0, \tag{4}$$

where $P(s)$ and $Q(s)$ are polynomials of s and given as follows:

$$\begin{aligned} P(s) &= p_7s^7 + p_6s^6 + p_5s^5 + p_4s^4 + p_3s^3 + p_2s^2 + p_1s \\ Q(s) &= q_4s^4 + q_3s^3 + q_2s^2 + q_1s + q_0, \end{aligned} \tag{5}$$

where p and q coefficients depending on parameters of the MG are given in (15) of Appendix.

3. Delay margin computation using direct method

The objective of the stability analysis of time-delayed systems is to determine if the system stability is dependent on the delay or not. If the system is stable for all finite delays, then the system is said to be delay-independent stable. For delay-dependent stable systems, however, the system stays stable for as long as $\tau < \tau^*$, where τ and τ^* denote the delay and stability delay margin, respectively. For $\tau > \tau^*$ cases, the system becomes unstable. This means that for the system to stay stable, the overall time delay should not be greater than the delay margin. To assess the stability of the MG, it is necessary to estimate delay margins for given system and controller parameters. For the system to be asymptotically stable, all roots of the characteristic equation in (4) must be located in the left half of the complex plane. Because of the exponential component of $e^{-s\tau}$, the characteristic equation in (4) is a transcendental equation, which means the polynomial might have an infinite number of finite roots. Subsequently, calculating their roots has become a difficult task. To calculate delay margin τ^* results for which the characteristic polynomial of (4) contains roots (if any) on the imaginary axis, however, computing all roots are not necessary.

The characteristic equation $\Delta(s, \tau) = 0$ is an inherent function of s and τ . It is assumed that the delay-free ($\tau = 0$) MG system is stable. This is a realistic assumption since the stability of the delay-free system could be assured by the appropriate selection of the system and controller parameters. Assume that for some finite value of τ , $\Delta(s, \tau) = 0$ contains a root on the imaginary axis at $s = j\omega_c$. Meanwhile, complex roots perpetually occur as a complex conjugate symmetry, the equation $\Delta(-s, \tau) = 0$ would consist the similar root at $s = j\omega_c$ for the same time delay τ . Hence, the task is now reduced to finding τ such that $\Delta(s, \tau) = 0$ and $\Delta(-s, \tau) = 0$ have the same root at $s = j\omega_c$. This consideration is expressed as follows:

$$\begin{aligned} P(j\omega_c) + Q(j\omega_c)e^{-j\omega_c\tau} &= 0 \\ P(-j\omega_c) + Q(-j\omega_c)e^{j\omega_c\tau} &= 0. \end{aligned} \tag{6}$$

By eliminating the exponential $e^{-s\tau}$ and $e^{s\tau}$ terms in (6), the following augmented characteristic equation of ω_c^2 is obtained.

$$\begin{aligned} W(\omega_c^2) &= P(j\omega_c)Q(-j\omega_c) - Q(j\omega_c)P(-j\omega_c) = 0 \\ &= m_{14}\omega_c^{14} + m_{12}\omega_c^{12} + m_{10}\omega_c^{10} + m_8\omega_c^8 + m_6\omega_c^6 + m_4\omega_c^4 + m_2\omega_c^2 + m_0 = 0. \end{aligned} \tag{7}$$

The augmented characteristic equation coefficients in terms of the coefficients of $P(s)$ and $Q(s)$ polynomials are provided in (16) of Appendix. When the transcendental term is removed from the characteristic equation in (4), the resulting equation is a regular polynomial represented in (7). The magnitude of the purely imaginary

roots $s = \pm j\omega_c$ of the original characteristic equation in (4) is precisely equal to the positive real roots in ω_c (7). Finding positive real roots of (7) is significantly simpler than computing imaginary roots of (4). Depending on the roots of (7), two stability occurrences can be witnessed. Those are as follows:

- i) If the augmented characteristic equation of (7) does not have any positive real roots for all finite delays $\tau \geq 0$ the system is said to be *delay – independent stable*. This implies that all the roots of (4) are in the left half stable plane for all finite delays $\tau \geq 0$.
- ii) If the augmented characteristic equation of (7) has at least one positive real root, the system is then said to be *delay – dependent stable*. This case indicates that roots of (4) cross the imaginary axis at $s = \pm j\omega_c$ for a finite stability delay margin τ^* .

For the positive real root $j\omega_c$ of the augmented characteristic equation in (7), using the characteristic equation of (4), an analytical formula could be derived to compute the stability delay margin of τ^* as follows [25, 31]:

The positive real root of the augmented polynomial of $W(\omega_c^2)$ is first substituted into (4)

$$\Delta(j\omega_c, \tau^*) = P(j\omega_c) + Q(j\omega_c)e^{-j\omega_c\tau^*} = 0 . \tag{8}$$

Next using the Euler identity of $e^{-j\omega_c\tau^*} = \cos(\omega_c\tau^*) - j \sin(\omega_c\tau^*)$ in (8) the exponential term is expressed as

$$e^{-j\omega_c\tau^*} = -\frac{P(j\omega_c)}{Q(j\omega_c)} = \cos(\omega_c\tau^*) - j \sin(\omega_c\tau^*) . \tag{9}$$

From the expression in (9), it is clear that

$$\begin{aligned} \cos(\omega_c\tau^*) &= \operatorname{Re} \left[-\frac{P(j\omega_c)}{Q(j\omega_c)} \right], \sin(\omega_c\tau^*) = \operatorname{Im} \left[\frac{P(j\omega_c)}{Q(j\omega_c)} \right] \\ \operatorname{Tan}(\omega_c\tau^*) &= \frac{\operatorname{Im} \left[\frac{P(j\omega_c)}{Q(j\omega_c)} \right]}{\operatorname{Re} \left[-\frac{P(j\omega_c)}{Q(j\omega_c)} \right]} . \end{aligned} \tag{10}$$

Finally, from (10), a general formula for the stability delay margin is determined as

$$\tau^* = \frac{1}{\omega_c} \operatorname{Tan}^{-1} \left(\frac{\operatorname{Im} \left[\frac{P(j\omega_c)}{Q(j\omega_c)} \right]}{\operatorname{Re} \left[-\frac{P(j\omega_c)}{Q(j\omega_c)} \right]} \right) + \frac{2r\pi}{\omega_c} , r = 0, 1, 2, \dots, \infty . \tag{11}$$

By substituting the polynomials $P(j\omega_c)$ and $Q(j\omega_c)$ into (11), the following formula for the stability delay margin of the MG-VI system is derived:

$$\tau^* = \frac{1}{\omega_c} \operatorname{tan}^{-1} \left(\frac{t_{11}\omega_c^{11} + t_9\omega_c^9 + t_7\omega_c^7 + t_5\omega_c^5 + t_3\omega_c^3 + t_1\omega_c}{t_{10}\omega_c^{10} + t_8\omega_c^8 + t_6\omega_c^6 + t_4\omega_c^4 + t_2\omega_c^2} \right) + \frac{2r\pi}{\omega_c} , r = 0, 1, 2, \dots, \infty . \tag{12}$$

The corresponding coefficients are given in (17) of Appendix.

Furthermore, the root tendency (RT) at $s = j\omega_c$ must be defined. The RT is calculated using root sensitivity, which allows us to see if the root of (4) crosses the imaginary axis when τ increases or not. Nonzero sensitivity is required to cross the imaginary axis, as seen below.

$$\operatorname{Re} \left[\frac{ds}{d\tau} \right]_{s=j\omega_c} \neq 0 , \tag{13}$$

where $\text{Re}(\bullet)$ stands for the real part of a complex variable. The sign of root sensitivity is referred to as RT [25, 27, 31].

$$RT|_{s=j\omega_c} = \text{sgn} \left\{ \text{Re} \left[\frac{ds}{d\tau} \right]_{s=j\omega_c} \right\} = \text{sgn} [W'(\omega_c^2)] , \quad (14)$$

where the prime denotes the derivative of (7) with respect to ω_c^2 . The derivation of the RT expression of (14) is provided in [27, 31]. The RT derivation of (14) allows a way to figure out which way the roots are moving as τ rises from $\tau_1 = \tau^* - \Delta\tau$ to $\tau_1 = \tau^* + \Delta\tau$, $0 < \Delta\tau \ll 1$. When $RT = +1$, the roots at $s = \pm j\omega_c$ cross the imaginary axis towards the right half plane to become unstable. When $RT = -1$, on the other hand, the roots migrate towards the stable left half plane.

4. Results and discussion

The parameters of the MG-VI system used for this study are given in [3]. Using time-domain simulations [40] and the QPmR algorithm [41], the accuracy of theoretical delay margins for various PI controller gains is validated.

$$M = 0.164, D = 0.016, R = 2.4, \beta = 0.99, T_{PV} = 1.9, T_W = 1.4, T_g = 0.1, T_t = 0.4, T_{INV} = 10s.$$

4.1. Illustration of delay margin computation

The impact of VI the stability delay margins of MGs for a wide range of PI controller gains is investigated. The disturbance effects of the RESs and loads are considered load variation ($\Delta P_L = 0.1pu$), wind speed variation ($\Delta P_W = 0.01pu$), and solar radiation variation ($\Delta P_{PV} = 0.01pu$). The computational process of the stability delay margin and verification study include the following next five presented in the following for ($K_P = 0.2, K_I = 0.2$):

Step 1: Obtain the characteristic equation of (4) for the chosen system parameters and PI controller gains. The characteristic polynomial is found to be:

$$\Delta(s, \tau) = \left(\begin{array}{l} (0.4188s^7 + 6.2457s^6 + 24.1830s^5 + 65.9101s^4 + 69.8379s^3 + 29.00752s^2 + 3.9184s) \\ + (12.6403s^4 + 29.5860s^3 + 23.2658s^2 + 6.7954s + 0.4752) e^{-s\tau} \end{array} \right) = 0 .$$

Step 2: Determine the augmented characteristic equation of (7). This equation is as follows:

$$W(\omega_c) = \left(\begin{array}{l} 0.1754\omega_c^{14} + 18.7541\omega_c^{12} - 180.0001\omega_c^{10} \\ + 1165.6\omega_c^8 + 955.9235\omega_c^6 + 142.9144\omega_c^4 \\ - 8.7113\omega_c^2 - 0.2258 \end{array} \right) = 0 .$$

Step 3: Determine all positive real roots, $\omega_c > 0$, of the augmented polynomial found in **Step 2**. The corresponding positive real root is computed as $\omega_c = 0.2462rad/s$. Note that all the remaining roots of (7) are either complex or real negative.

Step 4: For the root $\omega_c = 0.2462rad/s$ found in **Step 3**, compute stability delay margin using (12) and RT using (14). The delay margin and RT are obtained as

$$\tau^* = \frac{1}{\omega_c} \tan^{-1} \left(\frac{-5.29\omega_c^{11} + 130.64\omega_c^9 + 546.84\omega_c^7 + 379.76\omega_c^5 + 72.76\omega_c^3 + 1.86\omega_c}{66.56\omega_c^{10} - 260.11\omega_c^8 - 327.47\omega_c^6 - 115.7\omega_c^4 - 12.84\omega_c^2} \right) = 8.77s$$

$$RT|_{s=j\omega_c} = \text{sgn} [W'(\omega_c^2)] = +1 .$$

Step 5: Confirm the accuracy of the delay margin using time domain simulation and QPMR algorithm.

4.2. Delay margin results of MG with VI control for different controller gains

Table 1 shows stability delay margins over a range of $K_P = 0.1-1$ and $K_I = 0.1-1$ for the MG without VI. The numbers in the table indicated with an asterisk (*) show that the system is unstable for $\tau = 0$, implying that the delay-free system is unstable for the corresponding parameter values. The impacts of VI control on the stability delay margin are explored by choosing the virtual inertia and damping parameters as ($K_{VI} = 1.6, D_{VI} = 1.2$). For the same set of PI controller gains as in Table 1, stability delay margins are shown in Table 2.

Table 1. Stability delay margin values for different PI controller parameters of the MG without VI ($K_{VI} = 0, D_{VI} = 0$).

τ^* (s)	K_I									
K_P	0.1	0.2	0.3	0.4	0.5	0.6	0.7	0.8	0.9	1
0.1	7.221	3.333	1.988	1.252	0.709	0.307	0.128	0.031	*	*
0.2	7.490	3.438	2.005	1.136	0.441	0.248	0.143	0.071	0.018	*
0.3	6.867	0.627	0.450	0.336	0.250	0.181	0.125	0.078	0.039	0.005
0.4	0.331	0.292	0.251	0.211	0.172	0.135	0.101	0.070	0.043	0.017
0.5	0.221	0.198	0.174	0.150	0.126	0.103	0.080	0.059	0.039	0.020
0.6	0.160	0.145	0.128	0.112	0.096	0.079	0.063	0.048	0.033	0.019
0.7	0.122	0.110	0.098	0.086	0.074	0.061	0.049	0.038	0.026	0.015
0.8	0.094	0.085	0.075	0.066	0.057	0.047	0.038	0.029	0.020	0.011
0.9	0.073	0.066	0.058	0.051	0.043	0.036	0.028	0.021	0.013	0.006
1	0.057	0.051	0.045	0.039	0.033	0.026	0.020	0.014	0.008	0.002

Table 2. Stability delay margin values for different PI controller parameters of the MG with VI ($K_{VI} = 1.6, D_{VI} = 1.2$).

τ^* (s)	K_I									
K_P	0.1	0.2	0.3	0.4	0.5	0.6	0.7	0.8	0.9	1
0.1	27.277	8.631	4.249	2.705	1.905	1.404	1.051	0.782	0.569	0.402
0.2	28.003	8.769	4.350	2.787	1.969	1.450	1.080	0.795	0.572	0.409
0.3	28.517	8.590	4.246	2.714	1.898	1.366	0.972	0.671	0.475	0.354
0.4	28.777	7.942	3.834	2.381	1.551	0.894	0.560	0.427	0.343	0.280
0.5	28.713	0.687	0.587	0.508	0.442	0.386	0.337	0.294	0.256	0.222
0.6	0.389	0.368	0.344	0.320	0.295	0.271	0.246	0.223	0.200	0.179
0.7	0.283	0.269	0.254	0.239	0.224	0.208	0.193	0.177	0.162	0.147
0.8	0.221	0.211	0.200	0.190	0.179	0.168	0.156	0.145	0.134	0.123
0.9	0.179	0.171	0.163	0.155	0.147	0.138	0.129	0.121	0.112	0.104
1	0.148	0.142	0.136	0.129	0.122	0.115	0.109	0.102	0.095	0.088

It is clear from Tables 1 and 2 that with the integration of the virtual inertia and damping into the MG system, stability delay margin values considerable increase for all selected PI controller gains. For example, as seen in Table 1, for the controller gains of ($K_P = 0.2, K_I = 0.2$), the delay margin is computed as $\tau^* = 3.438s$ when the VI control loop is not used ($K_{VI} = 0, D_{VI} = 0$). The stability delay margin is determined as $\tau^* = 8.77s$ when the VI control with the parameters of ($K_{VI} = 1.6, D_{VI} = 1.2$) is implemented. This is a significant enhancement in the delay margin and in the stability of the MG system. Tables 1 and 2 also show that such an enhancement is achieved for all selected PI controller gains. Note that larger delay margins indicate

more stable MGs. Moreover, delay margins in Tables 1 and 2 illustrate that, with an increase in K_I , the delay margin τ^* decreases when K_P is kept constant. This justifies that an increase in K_I leads to a less stable MG system. For fixed K_I , the impact of K_P on delay margin consists of two trends. The delay margin increases with a rise in K_P for the smaller values of K_P . However, τ^* decreases for the larger values of K_P for all quantities of K_I . Furthermore, for the larger values of K_P , a small increase in K_P may cause a significant decrease in τ^* when K_I is fixed. When K_P is held constant, the data from both tables show that when K_I is increased, τ^* decreases. This explains why a rise in K_I causes the system to become less stable.

As shown in Table 2, stability delay margins significantly increase when the VI control is integrated into the MG. It is also essential to investigate the individual impact of VI control parameters, virtual inertia and damping, on the stability delay margin. For that purpose, firstly, virtual damping values are fixed at ($D_{VI} = 0.5, D_{VI} = 1.0$ and $D_{VI} = 1.5$) and the effect of virtual inertia on the stability delay margin is examined for the virtual inertia varying in an interval of $K_{VI} \in [0 - 2]$ and PI controller gains of ($K_P = 0.2, K_I = 0.2$). As seen in Figure 4, the stability delay margin rises with an increase in virtual inertia for all virtual damping values. Secondly, for the three different fixed virtual inertia values ($K_{VI} = 0.5, K_{VI} = 1.0$ and $K_{VI} = 1.5$), stability delay margins are computed for virtual damping changing in an interval $D_{VI} \in [0.1-2]$ for the same PI controller gains of ($K_P = 0.2, K_I = 0.2$). The stability delay margin increases as the virtual damping parameter increases, as displayed in Figure 5. These results indicate that the virtual inertia and damping values significantly increase the stability margin of MG system, emphasizing the positive impacts of the VI control loop on the stability of the MG system.

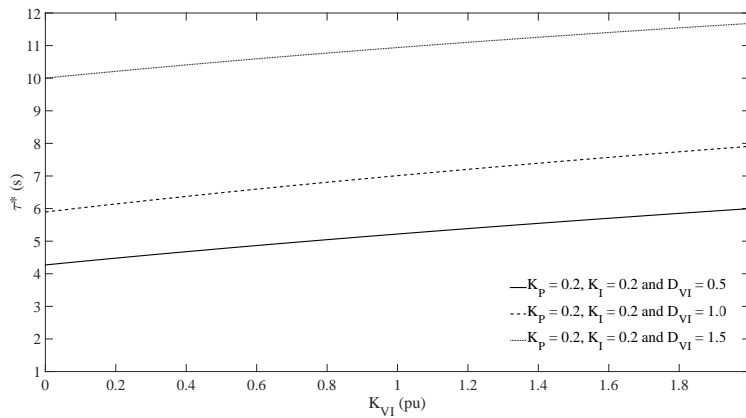


Figure 4. The impact of virtual inertia on the marginal time delay values.

The verification studies by both QPmR algorithm and time-domain simulations are implemented to prove the accuracy of stability delay margins for the controller gains of ($K_P = 0.2, K_I = 0.2$) and the VI controller parameters of ($K_{VI} = 1.6, D_{VI} = 1.2$). For these parameters, the theoretical delay margin is computed as $\tau^* = 8.77s$ using the direct method as shown in Table 2. Figure 6 illustrates frequency responses for a small disturbance in the load demand and complex root distributions of the MG system for three different time delays, $\tau^* = 8s, \tau^* = 8.77s$ and $\tau^* = 10s$. As shown in Figure 6a, when the time delay is less than the delay margin $\tau = 8s < \tau^* = 8.77s$, all the dominant poles of the MG-VI system computed by the QPmR algorithm are in the stable left half plane of the complex plane, indicating that the system is stable. The frequency response shown in the right-bottom corner of Figure 6a also proves that the MG-VI system is stable due to the decaying oscillations in the frequency response. Recall that the system should be marginally stable for ($\tau^* = 8.77s$).

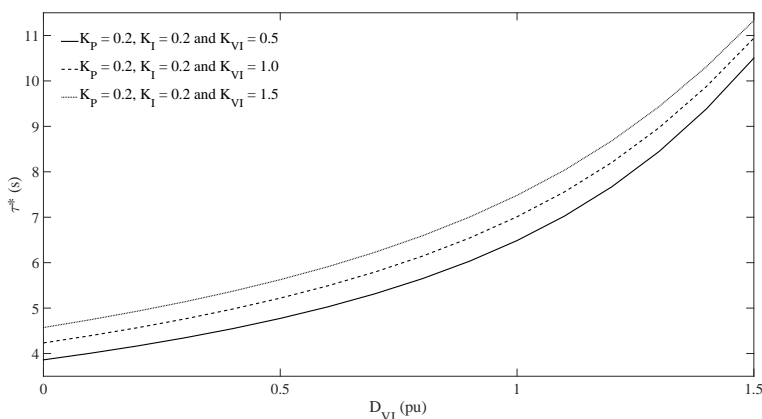


Figure 5. The impact of virtual damping on the marginal time delay values.

Figure 6b shows that the MG-VI system has a pair of complex conjugate roots on the imaginary axis and sustained frequency oscillations are observed, proving the marginal stability. Moreover, the complex roots on the imaginary axis, $s = \pm j\omega_c = \pm j0.2462 \text{ rad/s}$ computed by the direct method is exactly the same as one determined by the QPmR algorithm as shown at top-right corner of Figure 6b. Finally, when the time delay is larger than the delay margin ($\tau^* = 8.77s < \tau = 10s$), the MG-VI system has a pair of complex poles in the right-half plane of the complex plane and the system becomes unstable due to the growing oscillations in the frequency response as shown in Figure 6c.

Finally, simulation studies are carried out to emphasize the stabilizing effect of virtual inertia and damping on the MG system as given in Figure 7 that compares frequency responses of the MG system with and without VI control loop. Recall that for the MG without VI, the stability delay margin is $\tau^* = 3.44s$ for $K_P = 0.2$, $K_I = 0.2$ as shaded in Table 1 and the system is marginally stable as depicted in Figure 7. When a VI control loop is integrated into the MG, oscillations in the system frequency response are promptly dampened, and the transient dynamics are greatly enhanced. As shown in Figure 7, the performance criteria such as settling time, overshoots, and undershoots have significantly improved.

5. Conclusion

This paper has investigated the effects of VI control on stability delay margins of MGs. An analytical method not using any approximations has been utilized to evaluate the delay-dependency of stability and to calculate delay margins. Stability delay margins have been calculated for a wide range controller gains. The results show that theoretical delay margins are exactly the same as those by simulations and the QPmR algorithm. From the results, the following comments and observations could be made:

- i)* For all PI controller gains, with integration of VI control to the MG system, stability delay margins have been significantly enhanced.
- ii)* The destabilizing of time delays in MGs could be reduced with the use of VI control.
- iii)* A better frequency response could be obtained in MGs with time delays and RESs.
- iv)* Stability delay margins decrease with an increase in the controller gain. Furthermore, a small rise in integral controller gain may lead to a steep decline in the delay margin.

The computation of all stabilizing controller gains for MGs using stability boundary method and robust delay-dependent stability analysis are put in perspective as future work.

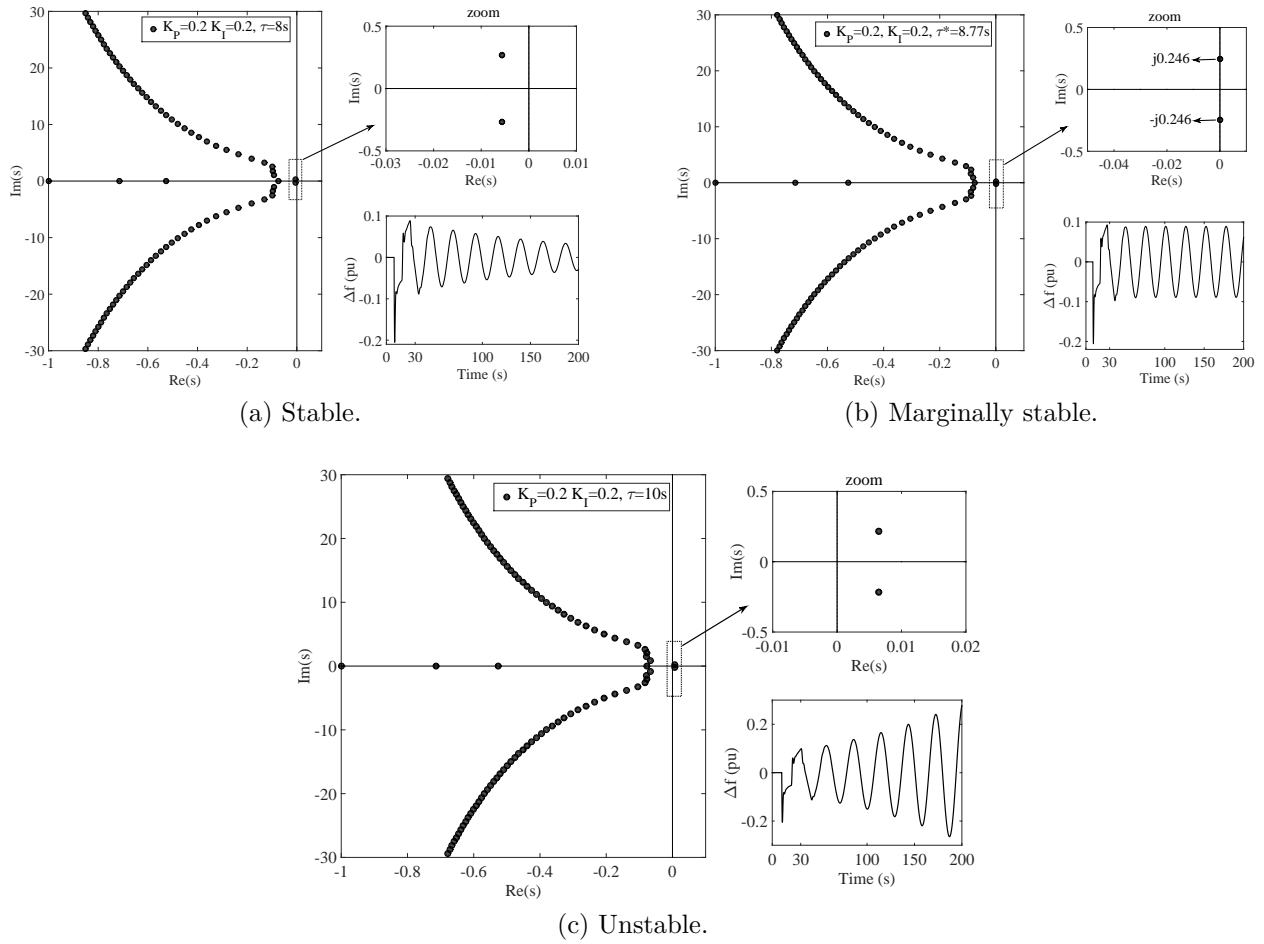


Figure 6. Dominant roots distribution and frequency responses.

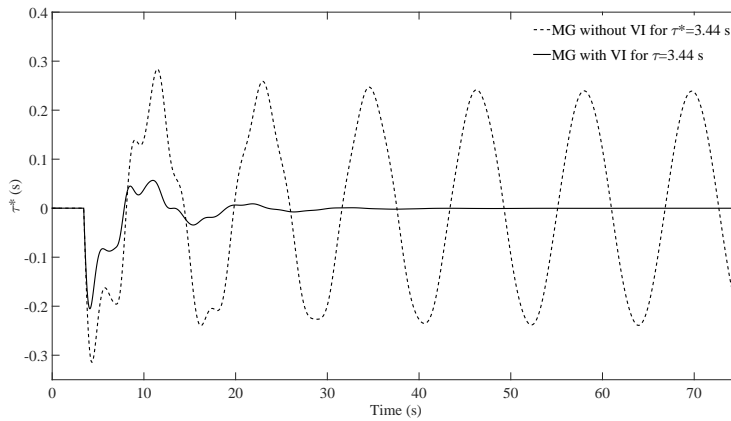


Figure 7. The comparison of frequency responses of the MG with/without VI for $K_P = 0.2, K_I = 0.2$.

References

- [1] Bevrani H, Ise T, Miura Y. Virtual synchronous generators: A survey and new perspectives. International Journal of Electrical Power & Energy Systems 2014; 54: 244-254. doi: 10.1016/j.ijepes.2013.07.009

- [2] Zamora R, Srivastava AK. Controls for microgrids with storage: Review, challenges, and research needs. *Renewable and Sustainable Energy Reviews* 2010; 14 (7): 2009-2018. doi: 10.1016/j.rser.2010.03.019
- [3] Kerdphol T, Rahman FS, Watanabe M, Mitani Y, Turschner D et al. Enhanced virtual inertia control based on derivative technique to emulate simultaneous inertia and damping properties for microgrid frequency regulation. *IEEE Access* 2019; 7: 14422-14433. doi: 10.1109/ACCESS.2019.2892747
- [4] Tamrakar U, Shrestha D, Maharjan M, Bhattarai BP, Hansen TM et al. Virtual inertia: Current trends and future directions. *Applied Sciences* 2017; 7 (7): 654. doi: 10.3390/app7070654
- [5] Bevrani H. *Robust power system frequency control*. New York, NY, USA: Springer, 2014.
- [6] Beck HP, Hesse R. Virtual synchronous machine. In: *2007 9th International Conference on Electrical Power Quality and Utilisation*; Barcelona, Spain; 2007. pp. 107-112.
- [7] Driesen J, Visscher K. Virtual synchronous generators. In: *2008 IEEE Power and Energy Society General Meeting - Conversion and Delivery of Electrical Energy in the 21st Century*; Pittsburgh, PA, USA; 2008. pp. 1- 5.
- [8] Zhong QC, Weiss G. Synchronverters: Inverters that mimic synchronous generators. *IEEE Transactions on Industrial Electronics* 2011; 58 (4): 1259-1267. doi: 10.1109/TIE.2010.2048839
- [9] Sakimoto K, Miura Y, Ise T. Stabilization of a power system with a distributed generator by a Virtual Synchronous Generator function. In: *8th International Conference on Power Electronics - ECCE Asia*; Jeju, South Korea; 2011. pp. 1498-1505.
- [10] Rodriguez P, Candela I, Luna A. Control of PV generation systems using the synchronous power controller. In: *2013 IEEE Energy Conversion Congress and Exposition*; Denver, CO, USA; 2013. pp. 993-998.
- [11] Abubakr H, Mohamed TH, Hussein MM, Guerrero JM, Agundis-Tinajero G. Adaptive frequency regulation strategy in multi-area microgrids including renewable energy and electric vehicles supported by virtual inertia. *International Journal of Electrical Power and Energy Systems* 2021; 129: 106819. doi: 10.1016/j.ijepes.2021.106814
- [12] Rafiee A, Batmani Y, Ahmadi F, Bevrani H. Robust load-frequency control in islanded microgrids: virtual synchronous generator concept and quantitative feedback theory. *IEEE Transactions on Power Systems* 2021; 36 (6): 5408-5416. doi: 10.1109/TPWRS.2021.3077768
- [13] Magdy G, Ali H, Xu D. A new synthetic inertia system based on electric vehicles to support the frequency stability of low-inertia modern power grids. *Journal of Cleaner Production* 2021; 297: 126595. doi: 10.1016/j.jclepro.2021.126595
- [14] Liu R, Wang S, Liu G, Wen S, Zhang J et al. An improved virtual inertia control strategy for low voltage ac microgrids with hybrid energy storage systems. *Energies* 2022; 15 (2): 442. doi: 10.3390/en15020442
- [15] Alghamdi B, Cañizares C. Frequency and voltage coordinated control of a grid of AC/DC microgrids. *Applied Energy* 2022; 310: 118427. doi: 10.1016/j.apenergy.2021.118427
- [16] Sarojini RK, Palanisamy K, Tuglie ED. A fuzzy logic-based emulated inertia control to a supercapacitor system to improve inertia in a low inertia grid with renewables. *Energies* 2022; 15(4): 1333. doi: 10.3390/en15041333
- [17] Naduvathuparambil B, Valenti MC, Feliachi A. Communication delays in wide area measurement systems. In: *Proceedings of the Thirty-Fourth Southeastern Symposium on System Theory*; Huntsville, AL, USA; 2002. pp. 118-122.
- [18] Xie X, Xin Y, Xiao J, Wu J, Han Y. WAMS applications in Chinese power systems. *IEEE Power and Energy Magazine* 2006; 4 (1): 54 – 63. doi: 10.1109/MPAE.2006.1578532
- [19] Wu H, Tsakalis KS, Heydt GT. Evaluation of time delay effects to wide-area power system stabilizer design. *IEEE Transactions on Power Systems* 2004; 19 (4): 1935 - 1941. doi: 10.1109/TPWRS.2004.836272
- [20] Yu X, Tomovic K. Application of linear matrix inequalities for load frequency control with communication delays. *IEEE Transactions on Power Systems* 2004; 19 (3): 1508 - 1515. doi: 10.1109/TPWRS.2004.831670

- [21] Jiang L, Yao W, Wu QH, Wen JY, Cheng SJ. Delay-dependent stability for load frequency control with constant and time-varying delays. *IEEE Transactions on Power Systems* 2012; 27(2): 932-941. doi: 10.1109/TPWRS.2011.2172821
- [22] Zhang CK, Jiang L, Wu QH, He Y, Wu M. Further results on delay-dependent stability of multi-area load frequency control. *IEEE Transactions on Power Systems* 2013; 28 (4): 4465 - 4474. doi: 10.1109/TPWRS.2013.2265104
- [23] Gu K, Kharitonov VL, Chen J. *Stability of time-delay systems*. Boston, MA, USA: Birkhäuser, 2003.
- [24] Chen J, Gu G, Nett CN. A new method for computing delay margins for stability of linear delay systems. *Systems & Control Letters* 1995; 26 (2): 107-117. doi: 10.1016/0167-6911(94)00111-8
- [25] Walton KE, Marshall JE. Direct method for TDS stability analysis. *IEE Proceedings D - Control Theory and Applications* 1987; 134 (2): 101-107. doi: 10.1049/ip-d.1987.0018
- [26] Rekasius ZV. A stability test for systems with delays. In: *Joint Automatic Control Conference*; San Francisco, CA, USA; 1980. Paper No. TP9-A.
- [27] Olgac N, Sipahi R. An exact method for the stability analysis of time-delayed linear time-invariant (LTI) systems. *IEEE Transactions on Automatic Control* 2002; 47 (5): 793-797. doi: 10.1109/TAC.2002.1000275
- [28] Gündüz H, Sonmez Ş, Ayasun S. A comprehensive gain and phase margins-based stability analysis of micro-grid frequency control system with constant communication time delays. *IET Generation Transmission & Distribution* 2017; 11 (3): 719-729. doi: 10.1049/iet-gtd.2016.0644
- [29] Gündüz H, Sonmez Ş, Ayasun S. Gain and phase margins based stability analysis of micro grid systems with time delay by using Rekasius substitution. *Journal of the Faculty of Engineering and Architecture of Gazi University*, 2019; 34 (1): 553-567. doi: 10.17341/gazimmfd.416515
- [30] Erol H. Stability analysis of pitch angle control of large wind turbines with fractional order PID controller. *Sustainable Energy, Grids and Networks*, 2021; 26: 100430. doi: 10.1016/j.segan.2021.100430
- [31] Sönmez Ş, Ayasun S, Nwankpa CO. An exact method for computing delay margin for stability of load frequency control systems with constant communication delays. *IEEE Transactions on Power Systems* 2016; 31 (1): 370-377. doi: 10.1109/TPWRS.2015.2403865
- [32] Naveed A, Sönmez Ş, Ayasun S. Impact of electric vehicles aggregators with communication delays on stability delay margins of two-area load frequency control system. *Transactions of the Institute of Measurement and Control*, 2021; 9 (12): 2860-2871. doi: 10.1177/01423312211014420
- [33] Naveed A, Sönmez Ş, Ayasun S. Impact of load sharing schemes on the stability delay margins computed by Rekasius substitution method in load frequency control system with electric vehicles aggregator. *International Transactions on Electrical Energy Systems*, 2021; 31 (5): e12884. doi: 10.1002/2050-7038.12884
- [34] Zaman MSU, Bukhari SBA, Hazazi KM, Haider ZM, Haider R et al. Frequency response analysis of a single-area power system with a modified LFC model considering demand response and virtual inertia. *Energies* 2018; 11 (4): 787. doi: 10.3390/en11040787
- [35] Kerdphol T, Rahman FS, Watanabe M, Mitani Y. Robust virtual inertia control of a low inertia microgrid considering frequency measurement effects. *IEEE Access* 2019; 7: 57550 - 57560. doi: 10.1109/ACCESS.2019.2913042
- [36] Aluko AO, Carpanen RP, Dorrell DG, Ojo EE. Impact assessment and mitigation of cyber attacks on frequency stability of isolated microgrid using virtual inertia control. In: *2020 IEEE PES/IAS PowerAfrica*; Nairobi, Kenya; 2020. pp. 1-5.
- [37] Arani MFM, Mohamed YARI, El-Saadany EF. Analysis and mitigation of the impacts of asymmetrical virtual inertia. *IEEE Transactions on Power Systems* 2014; 29 (6): 2862 - 2874. doi: 10.1109/TPWRS.2014.2309675
- [38] Khan S, Bletterie B, Anta A, Gawlik W. On small signal frequency stability under virtual inertia and the role of PLLs. *Energies* 2018; 11 (9): 2372. doi: 10.3390/en11092372

- [39] Moradi MH, Amiri F. Virtual inertia control in islanded microgrid by using robust model predictive control (RMPC) with considering the time delay. *Soft Computing* 2021; 25 (8): 6653 - 6663. doi: 10.1007/s00500-021-05662-z
- [40] Simulink. Simulation and model-based design. Natick, MA, USA: MathWorks, 2019.
- [41] Vyhlídal T, Zítek P. Mapping based algorithm for large-scale computation of quasi-polynomial zeros. *IEEE Transactions on Automatic Control* 2009; 54 (1): 171-177. doi: 10.1109/TAC.2008.2008345
- [42] Rakhshani E, Remon D, Cantarellas AM, Garcia JM, Rodriguez P. Virtual synchronous power strategy for multiple HVDC interconnections of multi-area AGC power systems. *IEEE Transactions on Power Systems* 2017; 32 (3): 1665 - 1677. doi: 10.1109/TPWRS.2016.2592971
- [43] Rakhshani E, Rodriguez P. Inertia emulation in AC/DC interconnected power systems using derivative technique considering frequency measurement effects. *IEEE Transactions on Power Systems* 2017; 32 (5): 3338-3351. doi: 10.1109/TPWRS.2016.2644698

Appendix

$P(s)$ and $Q(s)$ polynomials of (4) coefficients are:

$$\begin{aligned}
 p_7 &= MRT_{INV}TgT_{PV}T_tTW \\
 p_6 &= RT_gT_{PV}T_t(MT_{INV} + MT_W + K_{VI}T_W + DT_{INV}T_W) + \\
 &\quad MT_{INV}T_W(RT_gT_{PV} + RT_gT_t + RT_{PV}T_t) \\
 p_5 &= RT_gT_t(MT_{INV} + MT_W + K_{VI}T_W + DT_{INV}T_W) + \\
 &\quad RT_gT_{PV}T_t(K_{VI} + M + DT_{INV} + DT_W + D_{VI}T_W) + \\
 &\quad MRT_{INV}(T_gT_{PV} + T_{PV}T_t) + MT_{INV}T_W(RT_g + RT_{PV} + RT_t) + \\
 &\quad RT_WT_{PV}(MT_t + MT_g + DT_tT_{INV}) + RT_WT_{PV}(DT_gT_{INV} + K_{VI}T_t + K_{VI}T_g) \\
 p_4 &= RT_{INV}(MT_t + MT_W + DT_tT_W) + T_tTW R(K_{VI} + M) + T_{INV}T_{PV}T_W + \\
 &\quad RT_gT_{PV}(K_{VI} + M + DT_{INV}) + (MRT_g + MRT_{PV})(T_{INV} + T_t + T_W) + \\
 &\quad (RT_g + RT_{PV})(K_{VI}T_t + K_{VI}T_W + DT_{INV}T_t + DT_{INV}T_W) + \\
 &\quad T_{PV}T_W R(D + D_{VI})(T_g + T_t) + RT_gT_t(D + D_{VI})(T_{PV} + T_W) \\
 p_3 &= D_{VI}RT_gT_t + (T_{PV} + T_W)D_{VI}RT_g + (T_{PV} + T_W)D_{VI}RT_t + (T_{PV}T_W)D_{VI}R + \\
 &\quad DRT_gT_t + (T_{INV} + T_{PV} + T_W)DRT_g + (K_{VI} + M)RT_g + (K_{VI} + M)RT_t + \\
 &\quad T_{INV}T_{PV} + T_{INV}T_W + (MT_{INV} + MT_{PV} + MT_W + J_{VI}T_{PV} + J_{VI}T_W)R + T_{PV}T_W + \\
 &\quad (T_{INV}T_{PV} + T_{INV}T_W + T_{PV}T_W)DR + (T_{INV} + T_{PV} + T_W)DRT_t \\
 p_2 &= (T_{INV} + T_g + T_{PV} + T_t + T_W)DR + T_{INV} + T_{PV} + T_W + \\
 &\quad (K_{VI} + M + D_{VI}T_g + D_{VI}T_{PV} + D_{VI}T_t + D_{VI}T_W)R \\
 p_1 &= DR + D_{VI}R + 1 \\
 q_4 &= \beta RK_P T_{INV} T_{pv} T_w \\
 q_3 &= [T_{INV} T_{pv} + T_{INV} T_w + T_{pv} T_w] \beta RK_P + \beta RK_I T_{INV} T_{pv} T_w \\
 q_2 &= [T_{INV} + T_{pv} + T_w] \beta RK_P + [T_{INV} T_{pv} + T_{INV} T_w + T_{pv} T_w] \beta RK_I \\
 q_1 &= \beta RK_P + [T_{INV} + T_{pv} + T_w] \beta RK_I \\
 q_0 &= \beta RK_I .
 \end{aligned} \tag{15}$$

The coefficients of $W(\omega_c^2)$ in (7) are given as:

$$\begin{aligned}
 m_{14} &= p_7^2 \\
 m_{12} &= p_6^2 - 2p_7p_5 \\
 m_{10} &= p_5^2 + 2p_7p_3 - 2p_6p_4 \\
 m_8 &= p_4^2 - q_4^2 - 2p_7p_1 + 2p_6p_2 - 2p_5p_3 \\
 m_6 &= p_3^2 - q_3^2 + 2p_5p_1 - 2p_4p_2 + 2q_4q_2 \\
 m_4 &= p_2^2 - q_2^2 - 2p_3p_1 - 2q_4q_0 + 2q_3q_1 \\
 m_2 &= p_1^2 - q_1^2 + 2q_2q_0 \\
 m_0 &= -q_0^2 .
 \end{aligned} \tag{16}$$

The coefficients of the formula in (12) are given as:

$$\begin{aligned}
 t_{11} &= -p_7q_4 \\
 t_{10} &= -p_7q_3 + p_6q_4 \\
 t_9 &= p_7q_2 - p_6q_3 + p_5q_4 \\
 t_8 &= p_7q_1 - p_6q_2 + p_5q_3 - p_4q_4 \\
 t_7 &= -p_7q_0 + p_6q_1 - p_5q_2 + p_4q_3 - p_3q_4 \\
 t_6 &= p_6q_0 - p_5q_1 + p_4q_2 - p_3q_3 + p_2q_4 \\
 t_5 &= p_5q_0 - p_4q_1 + p_3q_2 - p_2q_3 + p_1q_4 \\
 t_4 &= -p_4q_0 + p_3q_1 - p_2q_2 + p_1q_3 \\
 t_3 &= -p_3q_0 + p_2q_1 - p_1q_2 \\
 t_2 &= p_2q_0 - p_1q_1 \\
 t_1 &= p_1q_0 .
 \end{aligned} \tag{17}$$